Quasi-two-dimensional excitons in finite magnetic fields

Yu. E. Lozovik,[1] I. V. Ovchinnikov,[1] S. Yu. Volkov,[1] L. V. Butov,[2] and D. S. Chemla[2,3]
[1]*Institute of Spectroscopy, 142190, Moscow region, Troitsk, Russia*
[2]*Materials Sciences Division, E. O. Lawrence Berkeley National Laboratory, Berkeley, California 94720*
[3]*Department of Physics, University of California at Berkeley, Berkeley, California 94720*
(Received 12 October 2001; published 24 May 2002)

We present a theoretical and experimental investigation of the effects of a magnetic field on quasi-two-dimensional excitons. We calculate the internal structures and dispersion relations of spatially direct and indirect excitons in single and coupled quantum wells in a magnetic field perpendicular to the well plane. We find a sharp transition from a hydrogenlike exciton to a magnetoexciton with increasing the center-of-mass momentum at fixed weak field. At that transition the mean electron-hole separation increases sharply and becomes $\propto P/B_\perp$, where P is the magnetoexciton center-of-mass momentum and $B_\perp$ is the magnetic field perpendicular to the quantum well plane. The transition resembles a first-order phase transition. The magnetic-field–exciton momentum phase diagram describing the transition is constructed. We measure the magnetoexciton dispersion relations and effective masses in $GaAs/Al_{0.33}Ga_{0.67}As$ coupled quantum wells using tilted magnetic fields. The calculated dispersion relations and effective masses are in agreement with the experimental data. We discuss the impact of magnetic field and sample geometry on the condition for observing exciton condensation.

DOI: 10.1103/PhysRevB.65.235304 PACS number(s): 71.35.Ji, 71.35.Lk, 63.20.Ls

I. INTRODUCTION

The theory of Mott excitons in a magnetic field was first developed by Elliott and Loudon[1] and by Hasegawa and Howard,[2] who considered the case of exciton with zero center-of-mass (c.m.) momentum. The exciton dispersion relation, i.e., the influence of the exciton motion on its spectrum, was subsequently investigated in the high-magnetic field limit (when cyclotron energy is much larger than the Coulomb energy) in the cases of three-dimensional (3D) excitons,[3] 2D excitons in a perpendicular magnetic field,[4–6] and spatially indirect quasi-2D excitons also in a perpendicular magnetic field.[7]

The interest in this issue stems from the unique coupling between the exciton internal structure and c.m. motion induced by the magnetic field.[3–7] To illustrate this result let us consider a 2D exciton, made of an electron e and a hole h, free to move parallel to the $\{\hat{x},\hat{y}\}$ plane. In the absence of magnetic field they form a flat hydrogenic system with c.m. momentum $\mathbf{P}\in\{\hat{x},\hat{y}\}$. A high magnetic field applied perpendicular to the $\{\hat{x},\hat{y}\}$ plane, $\mathbf{B}=B_\perp\hat{z}$, changes this picture completely, forcing the electron and the hole to travel with the same velocity, $\mathbf{v}_g=\partial E_X/\partial\mathbf{P}$, in such a way that they produce on each other a Coulomb force that cancels exactly the Lorentz force, Fig. 1(a).[4,6] Applying this condition self-consistently determines 2D-magnetoexciton dispersion relation $E_X=E_X(\mathbf{P})$ and, in turn, its binding energy E_B and effective mass M_B. In the high-magnetic-field limit the problem can be solved analytically.[4]

For the following it is convenient to introduce four quantities: (i) the magnetic length $l_B=\sqrt{\hbar c/(eB_\perp)}$, (ii) the cyclotron energy $\hbar\omega_c=\hbar eB/(\mu c)$, (iii) the 3D-exciton Bohr radius $a_B=\varepsilon\hbar^2/(\mu e^2)$, and (iv) its binding energy $R_y=\mu e^4/(2\varepsilon^2\hbar^2)$; here, m_e, m_h, and $\mu=m_em_h/(m_e+m_h)$ are, respectively, the e and h effective masses and the e-h reduced mass. l_B and $\hbar\omega_c$ fix the magnetic length and energy scales, whereas a_B and R_y determine the Coulomb ones. In the following we measure the exciton energy from the semiconductor gap.

In the high-magnetic-field limit one can demonstrate analytically the following interesting results for 2D magnetoexcitons built up from e and h in the zeroth Landau levels (LL's) (Ref. 4): (1) The magnetoexciton dispersion relation is given by $E_X(P)=-E_Be^{-\beta}I_0(\beta)$, where $I_0(x)$ is the modified Bessel function and $\beta=[Pl_B/(2\hbar)]^2$. (2) The magnetoexciton binding energy is proportional to square root of $B_\perp$, $E_B=\sqrt{\pi/2}e^2/(\varepsilon l_B)\sim\sqrt{B_\perp}$. (3) For small momenta $Pl_B/\hbar\ll1$, the magnetoexciton dispersion is parabolic and is characterized by an effective magnetoexciton mass $M_B=(2^{3/2}\varepsilon\hbar^2)/(\pi^{1/2}e^2l_B)\sim\sqrt{B}_\perp$. (4) For a magnetoexciton with $P=0$ the magnetic length plays the role of the Bohr radius. (5) Magnetoexcitons with momentum $\mathbf{P}$ carry an electric dipole in the direction perpendicular to $\mathbf{P}$ whose magnitude $e\langle\mathbf{r}\rangle=e\langle\mathbf{r}_e-\mathbf{r}_h\rangle=e\hat{z}\times\mathbf{P}l_B^2/\hbar$ is proportional to P. This expression makes explicit the coupling between the c.m. motion and the internal structure. This coupling results in a curious property, called the electrostatic analogy: The dispersion $E_X(\mathbf{P})$ can be calculated from the expression of the Coulomb force between e and h as a function of $\langle\mathbf{r}\rangle$ and has the unusual consequence that the magnetoexciton mass and binding energy depend on the magnetic field only and are independent of m_e and m_h. Contrary to the e-h system at zero magnetic field (hydrogenic problem), all e-h pairs are bound states and there is no scattering state. At $Pl_B/\hbar\gg1$ the separation between e and h tends to infinity and the magnetoexciton energy tends toward the sum of the lowest e and h LL energies, i.e., $\frac{1}{2}\hbar\omega_c$. The theoretical magnetoexciton dispersion is shown in Fig. 1(c).

The internal structure and dispersion relation of the 2D magnetoexciton are qualitatively different from those of 2D

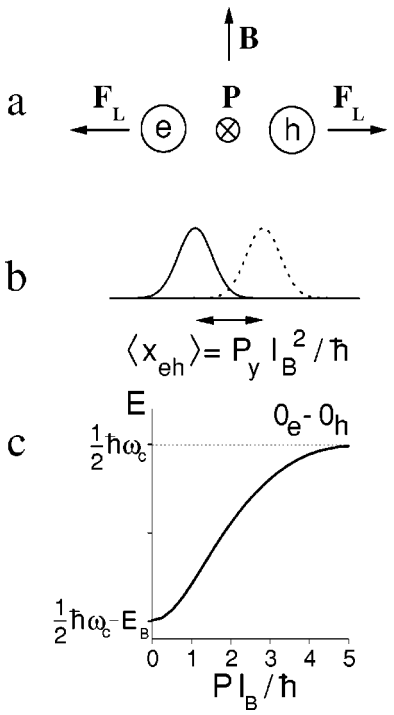

FIG. 1. Schematics showing (a) the coupling between the 2D-magnetoexciton center-of-mass and internal motions, (b) the separation between the electron and hole wave functions for 2D magnetoexcitons, and (c) calculated dispersions of 2D magnetoexciton in the high-magnetic-field limit.

excitons at zero magnetic field. This is clearly seen by comparing the lowest-energy states of these two limits which evolve into each other when B is varied: the magnetoexciton, which is built up from e and h in the zeroth LL's, and the 1s exciton at $B=0$. For the former, the dispersion relation is given above and is shown in Fig. 1(c) and $\langle \mathbf{r} \rangle = \hat{z} \times \mathbf{P} l_B^2/\hbar$. For the latter, the dispersion relation is quadratic $E_X(P) = P^2/2M - E_b$ and $\langle r \rangle = 0 \ \ \forall P$; here, $M = m_e + m_h$ is the exciton mass and E_b is the exciton binding energy which is equal to $4R_y$ for 2D excitons. Clearly the transition from the 2D exciton at zero magnetic field to the 2D magnetoexciton is nontrivial, and this is the subject of the present paper.

Experimentally, quasi-2D exciton systems are realized in two types of heterostructures: regular (single) quantum wells (SQW's) and coupled quantum wells (CQW's). As shown in Fig. 2, in the first case the e and h reside in the same layer and form spatially direct excitons, whereas in the second case the e and h are in two different layers separated by a distance d (along the growth direction $\hat{z}$) and form spatially indirect excitons. In this article we study the dispersion relations and internal structures of both spatially direct and indirect excitons in SQW's and CQW's for a wide range of magnetic fields perpendicular to the QW plane. We use a direct method for solving the Schrödinger equation in the imaginary time formalism and we identify two very distinct regimes. The first is realized for weak $B_\perp$ and small momenta P, where the e-h Coulomb attraction is dominant and the exciton structure is that of a strongly bound hydrogenic e-h state, only slightly modified by $B_\perp$. In the other regime, at

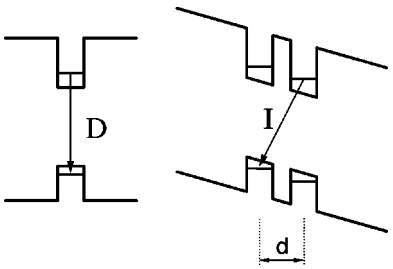

FIG. 2. Schematics showing the direct (D) and indirect (I) excitons in SQW's (left) and CQW's (right) with electron and hole residing either in the same layer or in layers separated by a distance d along the growth axis.

high $B_\perp$ or large P, the exciton structure is dominated by the interaction of each carrier with the magnetic field. It is essential to realize that the latter regime occurs for large values of P even at weak $B_\perp$, when the e-h separation in the $\{\hat{x},\hat{y}\}$ plane, $\langle \mathbf{r} \rangle = \hat{z} \times \mathbf{P} l_B^2/\hbar$, is large and the Coulomb interaction is small compared to the interaction with the magnetic field. From now on we will call the excitons in these regimes hydrogenlike excitons and magnetoexcitons, respectively. We find that for magnetic fields smaller than a critical value B_0 [see Eq. (12)] there is a sharp transition between these two regimes as P grows. At the transition point $P = P_{tr}(B_\perp)$ the exciton dispersion relation abruptly changes from a quadratic dependence, $E_X(P) \propto P^2$ for $P < P_{tr}(B_\perp)$, to being practically independent on P, $E_X(P) \approx \frac{1}{2}\hbar\omega_c$ for $P > P_{tr}(B_\perp)$. The origin of this transition is that the effective potential $U_{eff}(r)$ defining the internal exciton structure has two minima, one corresponding to the Coulomb attraction and the other induced by $B_\perp$, as sketched in Fig. 3(a). The separation between these minima is proportional to P. As illustrated in Fig. 3(a), when P increases (at fixed $B_\perp$) the energy of the Coulomb minimum increases and eventually crosses that of the magnetic minimum at the transition point $P = P_{tr}(B_\perp)$, where the exciton ground-state wave function jumps from the Coulomb minimum to the magnetic minimum (in the following the term ''ground state'' is used for the lowest-energy exciton state at any particular P). In the high-magnetic-field limit, defined by $E_b, E_B \ll \hbar\omega_c$, only the magnetoexciton regime exists and $\langle r \rangle = cP/(eB_\perp) \ \forall P$, whereas for intermediate fields the transition smears out into a crossover region. Following the evolution of the exciton dispersion as $B_\perp$ varies we also determine the variation of its effective mass, M_X. We find that the magnetic-field-induced enhancement of the effective mass is very different for spatially direct and indirect excitons, with a strong dependence on the spacing between the e layer and h layer, d. For example, when $B_\perp = 0 \rightarrow 10$ T the mass of the direct excitons, $d = 0$, is not much affected; conversely, for indirect excitons with $d = 11.5$ nm the mass increases by ~ 6 times. The calculated mass enhancement for indirect excitons with $d = 11.5$ nm is in agreement with the experimental data (see also Ref. 8).

The paper is organized as follows: In Sec. II we describe the basic quantum mechanics of e-h systems in magnetic fields and outline our numerical integration method. In Sec.

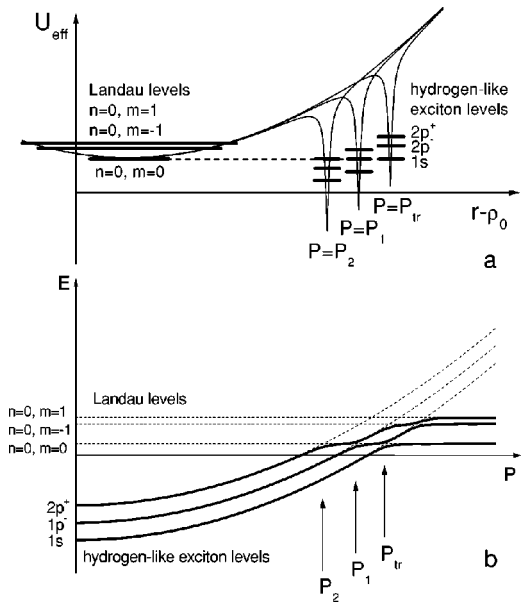

FIG. 3. (a) Schematics showing the variation of the effective potential at weak $B_\perp$ with increasing exciton momentum P. The Coulomb exciton levels slide along the magnetic parabola. $\rho_0 = cP/(eB_\perp)$ is the mean e-h separation for the magnetoexciton in the high-magnetic-field limit. (b) Schematic dispersions of the three lowest exciton states at weak $B_\perp$. The dotted parabolas and lines show, respectively, the three lowest hydrogenlike exciton states at $B=0$ and the three lowest sums of the e and h Landau-level energies which represent the three lowest magnetoexciton levels.

III we discuss the transition from the hydrogenlike exciton to the magnetoexciton. In Sec. IV we compare experimental data with theoretical results for the magnetoexciton dispersion relations and effective masses in finite $B_\perp$. Section V concludes our work.

II. QUASI-2D EXCITONS IN A MAGNETIC FIELD

The Hamiltonian of an interacting e-h pair in a magnetic field $\mathbf{B}$ is

$$\hat{H}=\sum_{i=e,h}\frac{1}{2m_i}\left(-i\hbar\frac{\partial}{\partial\mathbf{r}_i}+\frac{e_i}{c}\mathbf{A}(\mathbf{r}_i)\right)^2+V(\mathbf{r}_e-\mathbf{r}_h). \quad (1)$$

Here V is the e-h interaction and $\mathbf{A}$ is the vector potential generating $\mathbf{B}$. In the case of a 2D magnetoexciton it is convenient to distinguish the components of $\mathbf{B}$ parallel and perpendicular to the plane of the e-h motion: $\mathbf{B}=\mathbf{B}_\perp+\mathbf{B}_\parallel$, with $\mathbf{B}_\perp\|\hat{z}$ and $\mathbf{B}_\parallel=B_\parallel$ $(\hat{x}\cos\theta+\hat{y}\sin\theta)\in\{\hat{x},\hat{y}\}$, and to work in the gauge

$$\mathbf{A}(\mathbf{r})=\frac{1}{2}\mathbf{B}_\perp\times\mathbf{r}+zB_\parallel(\hat{x}\sin\theta-\hat{y}\cos\theta), \quad (2)$$

where $\mathbf{r}\in\{\hat{x},\hat{y}\}$. In what follows we consider for simplicity the case of deep and narrow QW's so that the e and h motion is approximately quasi two dimensional. They interact through the potential

$$V(r)=-\frac{e^2}{\varepsilon\sqrt{r^2+d^2}}. \quad (3)$$

For spatially indirect excitons, d is the distance between the centers of the e and h layers and $d=0$ for spatially direct exciton. Because the e-h Schrödinger equation is invariant under simultaneous translation of the e and h parallel to the $\{\hat{x},\hat{y}\}$ and the corresponding gauge transformation, there are 2D integrals of motion:[3,4]

$$\mathbf{P}_m=\mathbf{P}+\frac{ed}{c}\mathbf{B}_\parallel\times\hat{z},\quad \mathbf{P}=-i\hbar\frac{\partial}{\partial\mathbf{R}}+\frac{e}{2c}\mathbf{B}_\perp\times\mathbf{r}, \quad (4)$$

where $\mathbf{R}=(m_e\mathbf{r}_e+m_h\mathbf{r}_h)/M$ is the c.m. coordinate, $\mathbf{r}=\mathbf{r}_e-\mathbf{r}_h$ is the relative coordinate, $M=m_e+m_h$ is the e-h pair total mass, and we have introduced vector $\mathbf{P}$ which accounts for the effects of the perpendicular component of the magnetic field $\mathbf{B}_\perp$ only. The in-plane magnetic field $\mathbf{B}_\parallel$ has no effect on spatially direct (magneto)excitons, whereas for spatially indirect (magneto)excitons it shifts the dispersion curve by $(ed/c)\mathbf{B}_\parallel\times\hat{z}$ without changing its shape (to the second order in $B_\parallel$ and QW width).[8–11] Finally, since in the absence of an in-plane magnetic field the Hamiltonian is invariant under inversion, the dispersion relation depends only on $B_\perp$ and P^2.

By choosing wave functions of the form

$$\Psi_{\mathbf{P}_m}(\mathbf{R},\mathbf{r})=\exp\left[i\hbar^{-1}\mathbf{R}\left(\mathbf{P}_m+\frac{e}{2c\hbar}\mathbf{B}_\perp\times\mathbf{r}\right)\right]\psi_{\mathbf{P}_m}(\mathbf{r}), \quad (5)$$

one obtains the Hamiltonian for the relative motion wave function, $\psi_{\mathbf{P}_m}(\mathbf{r})$,[3]

$$\hat{H}=-\frac{\hbar^2}{2\mu}\Delta_\mathbf{r}+\frac{eB_\perp}{2c\eta}\hat{L}_z+\frac{P^2}{2M}+\frac{1}{2\mu}\left(\frac{eB_\perp}{2c}\right)^2r^2+\frac{e}{cM}\mathbf{B}_\perp\times\mathbf{P}\cdot\mathbf{r}+V(\mathbf{r}). \quad (6)$$

Here $\hat{L}_z=i\hbar\hat{z}\mathbf{r}\times\nabla_r$ is the angular momentum operator in the z direction, $\mu^{-1}=m_e^{-1}+m_h^{-1}$, and $\eta^{-1}=m_e^{-1}-m_h^{-1}$. The representation (6) deserves some comment. The second term describes the interaction of exciton magnetic dipole with the magnetic field and disappears when the carriers have the same masses. This is easy to understand, since in the c.m. coordinates, an electron and a hole with the same masses rotate around the c.m. at the same distance and, since they carry opposite charges, the total magnetic dipole of the system is zero. The fourth term, $(1/2\mu)[eB_\perp/(2c)]^2r^2$ is responsible for the Langevin diamagnetic shift and the fifth term expresses that an electric field $\boldsymbol{\mathcal{E}}=(cM)^{-1}\mathbf{B}_\perp\times\mathbf{P}$ appears in the c.m. frame of the e-h system moving in the magnetic field and interacts with the relative coordinate electric dipole $e\mathbf{r}$. This representation is helpful in the case of excitons with small momenta in weak $B_\perp$, when the Coulomb attraction dominates and determines the exciton internal structure. In that case, the terms linear and quadratic in $\mathbf{r}$ only slightly modify the exciton ground state and can be considered as perturbations.

It is also interesting to make the transformation,

$$\psi_{\mathbf{P}}(\mathbf{r}) = \exp\left(\frac{1}{2\hbar i}\frac{\mu}{\eta}\mathbf{P}\mathbf{r}\right)\phi_{\mathbf{P}}(\mathbf{r}+\boldsymbol{\rho}_0), \quad \boldsymbol{\rho}_0 = \frac{c}{eB}\hat{z}\times\mathbf{P}, \quad (7)$$

to obtain[3]

$$\hat{H} = -\frac{\hbar^2}{2\mu}\Delta_{\mathbf{r}} + \frac{eB_\perp}{2c\,\eta}\hat{L}_z + \frac{1}{2\mu}\left(\frac{eB_\perp}{2c}\right)^2 r^2 + V(\mathbf{r}+\boldsymbol{\rho}_0), \quad (8)$$

which is very useful in the opposite case of magnetoexcitons whose structure is mainly determined by the independent interaction between carriers and the magnetic field, and where it is the Coulomb interaction that can be considered as a perturbation.[3,4] This corresponds to large magnetic fields and/or large exciton momenta.

We concentrate on the magnetoexciton ground state. We determine numerically the solutions of the nonstationary Schrödinger equation in the imaginary time formalism. Any initial wave function $\psi(\mathbf{r},0)$ can be expressed on $\{\psi_j(\mathbf{r})\}$, the basis of eigenstates of the Hamiltonian (8), and its evolution in imaginary time t has the form

$$\psi(\mathbf{r},t) = \sum_j C_j e^{-E_j t/\hbar}\psi_j(\mathbf{r}), \quad (9)$$

where E_j, $j=1,2\ldots$, are the eigenvalues of Eq. (8). After each time step we normalize the wave function. Since the bound levels at fixed P are discrete, it follows that for times $t \gg \hbar(E_2-E_1)^{-1}$ all excited states, including those directly above the ground state, are exponentially eliminated and only the ground exciton state contributes to the wave function. In the calculations we used for units of length, energy, and momentum, respectively, $a_B/2$, $4R_y$ (i.e., the Bohr radius and the binding energy of a 2D direct exciton) and $P_0 = e^2M/(\varepsilon\hbar)$.

We performed the calculations for GaAs/$Al_{0.33}Ga_{0.67}$As CQW's studied experimentally in Refs. 8,10 and 12 with $\varepsilon = 12.1$ and $d = 11.5$ nm ($a_B/2 = 6.71\times10^{-7}$ cm, $4R_y = 17$ meV, and $P_0/\hbar = 3.62\times10^6$ cm^{-1}) and for AlAs/GaAs CQW's with $d = 3.5$ nm studied experimentally in Refs. 13 and 14.

III. TRANSITION FROM A HYDROGEN-LIKE EXCITON TO A MAGNETOEXCITON

Let us first discuss the case of weak magnetic fields. The "effective potential" $U_{eff}(r)$ of the e-h motion [last two terms in Eq. (8)] for $P \neq 0$ has the form shown in Fig. 3(a). The potential is anisotropic and has two minima separated by $\rho_0 = cP/(eB_\perp)$: The first is the Coulomb minimum corresponding to the fourth term of Eq. (8) and the second has its origin in the parabolic magnetic potential, third term of Eq. (8). Each minimum has its bound (or quasibound) levels. For large ρ_0 and weak magnetic fields the wave functions of the lowest levels in the minima have negligible overlap (see the Appendix) and the level splitting is small. Therefore, the corresponding energies, E_{Coul} for the Coulomb minimum and E_{magn} for the magnetic minimum, can be approximately calculated by perturbation theory. Within this approximation the exciton energy in the Coulomb minimum is $E_{Coul} = P^2/(2M) - E_b + \Delta E$, where E_b is the binding energy at $B=0$ and the correction ΔE comes from the Langevin shift [fourth term in Eq. (6)] and from the quadratic Stark shift $e\alpha\mathcal{E}^2$ [α is the exciton polarizability and $\boldsymbol{\mathcal{E}}$ the apparent field in the c.m. frame, fifth term in Eq. (6)]. The energy of the lowest level in the magnetic minimum can be estimated from the sum of the lowest e and h LL energies slightly perturbed by the Coulomb interaction $E_{magn} = \frac{1}{2}\hbar\omega_c - e^2/(\varepsilon\rho_0)$ [see Eq. (8) and Refs. 4 and 7].

Let us now consider the evolution of the exciton ground state for small $B_\perp$ as P increases. As long as $P < P_{tr}$, where

$$P_{tr} \approx \sqrt{2M\left(E_b + \frac{1}{2}\hbar\omega_c\right)}, \quad (10)$$

the Coulomb level E_{Coul} is lower in energy than the level in the magnetic minimum; i.e., the hydrogenlike exciton is the ground state and its wave function is almost that of the hydrogenlike exciton ground state in the absence of a magnetic field. When P increases the magnetic minimum gradually shifts away from the Coulomb minimum and the Coulomb level slides practically along the magnetic parabola, Fig. 3(a). When $P > P_{tr}$ the level in the magnetic minimum, i.e., the magnetoexciton, becomes the ground state. Therefore, at $P = P_{tr}$ there is a transition from the hydrogenlike exciton to the magnetoexciton. At the transition the e-h separation in the ground state abruptly increases to $\langle r\rangle = \rho_0 = cP/(eB_\perp)$; i.e., suddenly the size of the exciton blows up. Once the exciton has passed through the transition its energy changes only weakly as P continues to grow, Figs. 3(a) and 3(b). An interesting result is worth noting: the exciton momentum at the transition point is finite even for $B_\perp \to 0$; see Eq. (10). This limiting case is detailed in the Appendix.

The exciton spectrum in weak magnetic fields is illustrated in Fig. 3(b) and can be described qualitatively as follows. In the absence of a magnetic field the dispersion of the exciton ground state is quadratic, $E_X(\mathbf{P}) = P^2/(2M) - E_b$, and all the excited bound states have similar dispersion relation but with smaller binding energies as shown by the dotted parabolas in Fig. 3(b) which represent the first three hydrogenlike levels. For any weak magnetic field the magnetic minimum of the effective potential $U_{eff}(r)$ appears at $P \neq 0$ with its corresponding family of magnetoexciton states whose energies are $E(n,m) \approx \hbar\omega_c[n + 1/2(|m| + m\mu/\eta + 1)]$ and e-h separation $\langle r\rangle = \rho_0$.[4] The energies of the first three magnetoexciton levels are schematically represented by the dotted lines in Fig. 3(b). The levels of each family anticross because of tunneling between the wave functions, generating the dispersion curves $E_X(\mathbf{P})$ represented by the solid lines in Fig. 3(b). In particular for the lowest magnetoexciton level ($n=0$, $m=0$) and the lowest hydrogenlike exciton level the splitting is determined by the parameter δ (see the Appendix).

As shown in Fig. 4 the numerical solutions agree well with the above qualitative description. Here we present the evolution of $U_{eff}(r)$ for five values of $P = 0.1 \to 1.5$. The shift of the magnetic minimum and the transition from the hydrogenlike exciton ground state to magnetoexciton ground

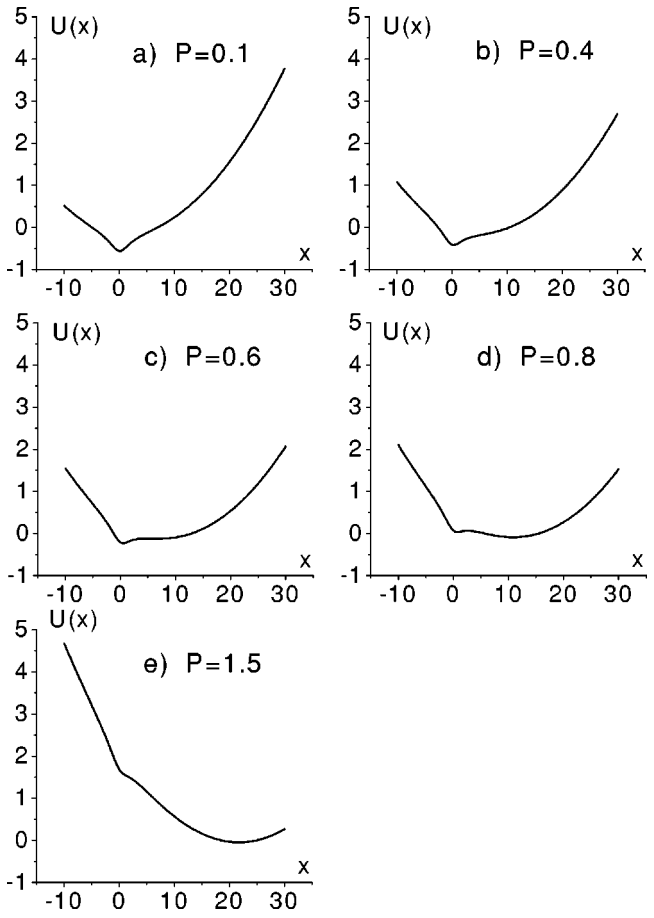

FIG. 4. (a) Calculated variation of the effective potential $U_{eff}(x)$ at $B_\perp = 2$ T with increasing exciton momentum P. The calculations are performed for indirect exciton in $GaAs/Al_{0.33}Ga_{0.67}As$ CQW with $d = 11.5$ nm. The units are given at the end of Sec. II.

state are clearly seen. In Fig. 5 we present the evolution of the dispersion relations of the ground state as $B_\perp$ increase. It shows that at weak fields the dispersion relation changes suddenly near the transition point $P = P_{tr}$, but is almost constant at $P > P_{tr}$. A sharp transition is observed up to $B_\perp \approx 1$ T for the indirect excitons [Fig. 5(a)] and up to $B_\perp \approx 8$ T for the direct excitons [Fig. 5(b)], which is discussed later in the section.

As already mentioned, in the c.m. frame the exciton experiences an electric field $\mathcal{E} = (cM)^{-1}\mathbf{B}\times\mathbf{P}$. In the hydrogenlike regime this produces a linear polarization of the exciton, with the appearance of an induced in-plane dipole $\mathbf{d} = e\langle\mathbf{r}\rangle = e\alpha\boldsymbol{\mathcal{E}} \propto P$. In the magnetoexciton regime, the average e-h separation $\langle r\rangle = \rho_0 = cP/(eB_\perp)$ also induces a dipole $\propto P$, with a different proportionality coefficient, however. The transition between the two types of electric field linear response is shown in Fig. 6, which presents the calculated $\langle\mathbf{r}(\mathbf{P})\rangle - \rho_0(\mathbf{P})$ for various $B_\perp$. At weak $B_\perp$ the transition from the hydrogenlike exciton regime (or weak-magnetic-field regime) to the magnetoexciton regime (or strong-magnetic-field regime) is characterized by the abrupt changes of $\langle\mathbf{r}(\mathbf{P})\rangle - \rho_0(\mathbf{P})$ corresponding to the sudden change of the exciton polarizability. In turn, the ground-state

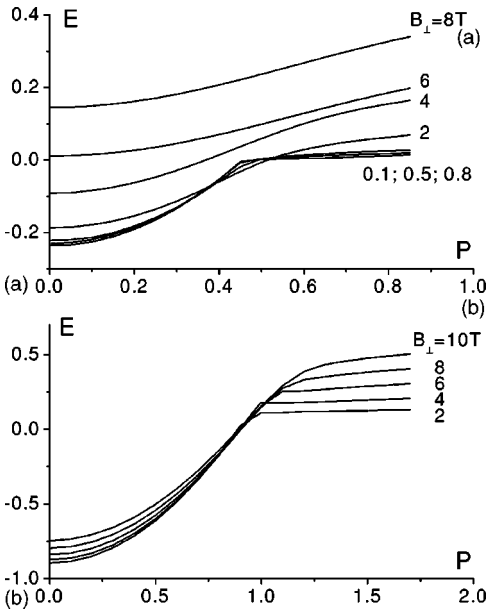

FIG. 5. Dispersion relations of spatially indirect (a) and direct (b) excitons in $GaAs/Al_{0.33}Ga_{0.67}As$ CQW's with $d = 11.5$ nm in various $B_\perp$. The units are given at the end of Sec. II. For the comparison with the experimental data see Fig. 11.

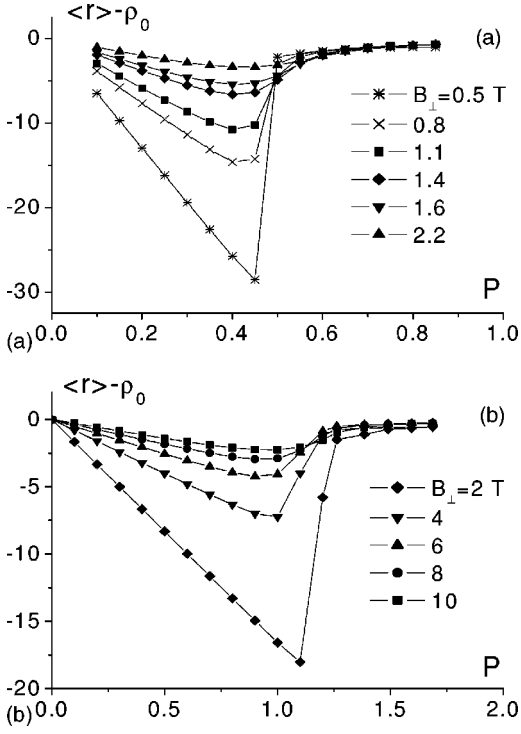

FIG. 6. The difference $\langle\mathbf{r}\rangle - \rho_0$ between the actual mean e-h separation $\langle\mathbf{r}\rangle$ and the mean e-h separation for the magnetoexciton in the high-magnetic-field limit $\rho_0 = cP/(eB_\perp)$ for indirect (a) and direct (b) excitons in various magnetic fields vs exciton momentum. The units are given at the end of Sec. II.

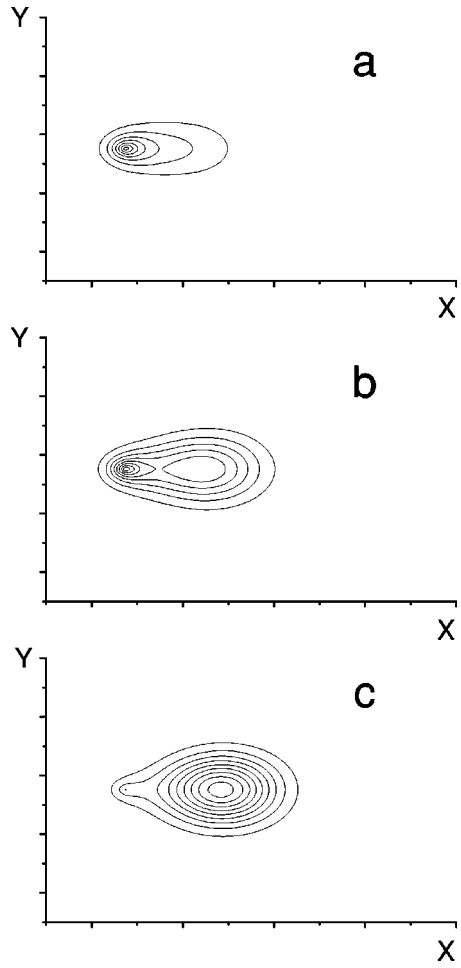

FIG. 7. Variation of the direct exciton ground-state wave function with increasing exciton momentum near the transition point at $B_\perp = 4$ T: (a) $P = 0.95P_0$, (b) $P = P_0$, and (c) $P = 1.05P_0$. The units are given at the end of Sec. II.

wave function suddenly changes from hydrogen like to magnetoexciton like at the transition, Fig. 7.

For $P > P_{tr}$ the exciton energy varies only slightly as P continues to increase. The metastable Coulomb level continues to slide up along the magnetic parabola until it disappears because of the strong anisotropy of the Hamiltonian (6) originating from the term $\propto \mathbf{r}$. In other words, the Coulomb minimum level disappears due to the ''autoionization'' of the hydrogenlike exciton by the strong (apparent) electric field $\boldsymbol{\mathcal{E}} = (cM)^{-1}\mathbf{B}\times\mathbf{P}$ into the magnetoexciton state with a large e-h separation. Note that for indirect excitons at higher P, the Coulomb minimum itself disappears [Fig. 4(e)]. The ''autoionization'' occurs when the characteristic anisotropy energy $2ea_B\mathcal{E}$ becomes comparable to E_b, i.e., for the momentum

$$P_{dsp}(B) = \frac{cME_b}{2ea_B B_\perp}. \tag{11}$$

For $P > P_{dsp}$ the bound hydrogenlike state disappears. Now it is simple to understand at which magnetic field e-h system makes the transition: At the transition point the metastable

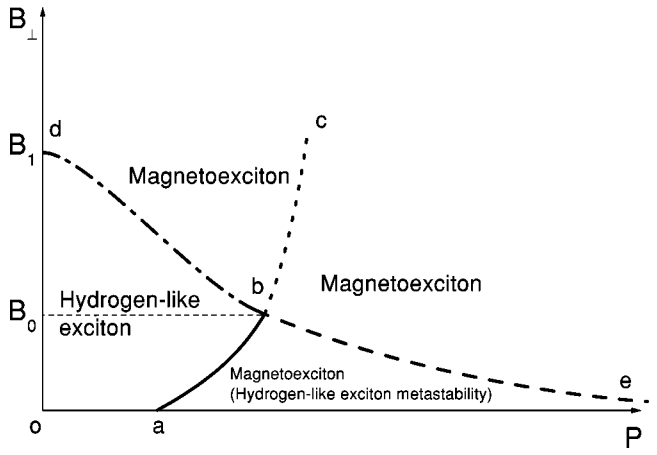

FIG. 8. Phase diagram for the exciton on the magnetic-field–exciton momentum plane. Line ab (excluding the point a itself) corresponds to the transition of the ground state from the hydrogenlike exciton to the magnetoexciton. $oabd$ is the region where the hydrogenlike exciton is the ground state. The magnetoexciton is the ground state in the remaining part of the plane. abe is the region where the metastable hydrogenlike level coexists with the magnetoexciton ground state. On the line bc the magnetoexciton dispersion has an inflection point.

Coulomb level must still exist or, in other words, P_{tr} must be smaller than P_{dsp}. Using Eqs. (10) and (11) this implies for the magnetic field that $B_\perp < B_0$, where

$$B_0 = \frac{cME_b}{2ea_B\sqrt{2M[E_b + \frac{1}{2}\hbar\omega_c(B_0)]}}. \tag{12}$$

At $B_\perp > B_0$ the exciton structure changes gradually as P increases, and, for example, in this case wave functions like the one shown in Fig. 7(b) cannot exist.

Now we can set the boundaries of the weak-magnetic-field regime defined as the region of the $\{P, B_\perp\}$ plane where the exciton ground state is hydrogenlike. Obviously, it occurs only for $P < P_{tr}, P_{dsp}$ and, in addition, it must also be limited by $B_\perp < B_1$ such that the cyclotron energy is much larger than the Coulomb energy $\hbar\omega_c(B_1) \gg E_b, E_B$.[3,4] This requirement terminates the weak-magnetic-field regime at $P \to 0$. As we already mentioned for $B_\perp > B_0$ there are no abrupt changes in the exciton structure in the $\{P, B_\perp\}$ plane and, therefore, when $B_1 > B_\perp > B_0$ only a smooth crossover between the weak- and strong-magnetic-field regimes exists.

These results are summarized in the $\{P, B_\perp\}$-plane phase diagram shown in Fig. 8. One can distinguish several regions, separated by various lines. Line ab (excluding the point a itself) corresponds to the hydrogenlike exciton $\to$magnetoexciton transition. The area $oabd$ is the weak-magnetic-field domain where the ground state is hydrogen like, whereas all the rest of the $\{P, B_\perp\}$ plane corresponds to the high-magnetic-field regime where the ground state is the magnetoexciton. abe is the region of coexistence of the metastable hydrogenlike level and the magnetoexciton ground state. The magnetoexciton dispersion relation has an inflection point on the line bc.

To illustrate the theory we now evaluate the critical parameters P_{tr} and B_0 for the spatially direct and indirect ($d=11.5$ nm) excitons in GaAs/$Al_{0.33}Ga_{0.67}$As CQW's. Equation (12) gives estimates of $B_0 \approx 1.4$ T for indirect exciton and $B_0 \approx 5.8$ T for direct exciton. More accurate values are obtained by noting again that for $B_\perp < B_0$ the exciton dispersion and internal structure exhibit the peculiarity at $P=P_{tr}$. Using this criterion in the numerical calculations we get $B_0 \approx 1$ T for the indirect exciton and $B_0 \approx 8$ T for the direct exciton. According to Eq. (10) as $B \to 0$ (point a in Fig. 8) $P_{tr} \approx 0.43 P_0$ for the indirect exciton and $P_{tr} = \sqrt{4\mu/M} P_0 \approx 0.95 P_0$ for the direct exciton. Both the estimates for B_0 and P_{tr} are in agreement with the numerical data as seen in Figs. 5 and 6.

So far we have considered the transition from hydrogenlike excitons to magnetoexcitons for the ideal model system of (separated) 2D spinless electrons and holes with isotropic parabolic dispersions. The theory does not include several aspects of real life semiconductor heterostructures, such as finite QW width effects, complex band structure effects, spin and in-plane localization effects. Although accounting in detail for these effects is beyond scope of our paper and deserves separate studies, it is worth discussing at least qualitatively how they affect the exciton dispersion and, in turn, the transition. As we will see the main theoretical results concerning the transition and the phase diagram are still valid for many real systems, in particular for high-quality GaAs/Al_xGa_{1-x}As QW and CQW structures with narrow QW's and high potential barriers.

Finite QW widths L modify the effect of both in-plane and perpendicular magnetic fields on (magneto)exciton dispersion. Up to second order in the in-plane magnetic field $B_\parallel$, the finite well width produces two effects: (1) diamagnetic shifts of electron and hole dispersions $\delta E_{dia} \propto L^2 B_\parallel^2$ (Ref. 15) and (2) van Vleck paramagnetism inducing a renormalization of electron and hole effective masses, $\delta M_{para} \propto L^4 B_\parallel^2$, along the $\hat{y} \perp B_\parallel$ direction.[10] These two contributions are negligible for narrow QW's and/or not too strong fields, i.e., when $L \lesssim l_{B_\parallel}$, where $l_{B_\parallel} = \sqrt{\hbar c/(eB_\parallel)}$ is the in-plane field magnetic length. Let us consider now the effect of a perpendicular magnetic field. When $L \neq 0$, $\mathbf{r}_z$, the mean separation between the electron and hole wave functions along $\hat{z}$, which is affected by the e-h Coulomb interaction, depends on the center-of-mass momentum P, thus changing the effect of $B_\perp$ on the dispersion law. A variational estimate of this effect shows that it is very weak for all $B_\perp$ considered in our work.

The electron and hole dispersions in real semiconductor QW structures are neither isotropic nor parabolic, and this modifies the exciton dispersion.[16] According to Kane's model, the conduction-band nonparabolicity $\delta m_e/m_e \sim \delta E/E$ causes negligible effects on the transition from hydrogenlike excitons to magnetoexcitons when $E_b, E_B \ll E_g$. This condition is satisfied for most semiconductors. The valence-band nonparabolicity and anisotropy originates mainly from the light-hole–heavy-hole coupling. It decreases with increasing light-hole–heavy-hole band splitting, δE_{LH-HH}, which varies as the square of the inverse of the QW thickness. Thus effects of the valence band nonparabolicity and anisotropy on the hydrogenlike exciton to magnetoexciton transition are negligible when $E_b, E_B \ll \delta E_{LH\text{-}HH}$.

In principle, the relative electron and hole spin orientation is determined by the interplay between electron and hole Zeeman splitting and e-h exchange interaction, with the later depending on e-h separation. At the transition from a hydrogenlike exciton to a magnetoexciton the mean in-plane e-h separation increases strongly and that could influence the relative electron-hole spin orientation by reducing the e-h exchange. For the case where the e-h exchange interaction and the electron and hole spin splittings are much smaller than E_b and E_B, a condition well satisfied for GaAs/Al_xGa_{1-x}As QW structures, the spin effects on the exciton dispersions and the transition can be neglected. Therefore, we do not consider the spin effects in this paper.

We now consider the effects of exciton localization by an in-plane random potential, due to unavoidable interface roughness, impurities, etc., on the transition from the compact hydrogenlike exciton, size $\approx a_B$, to the extended magnetoexciton, size $\approx \rho_0(P) = (cP)/(eB_\perp)$. The localization effects are negligible when (i) the (magneto)exciton momentum uncertainty $\hbar/l$ [l is the mean free path of the (magneto)exciton] is much smaller than P_{tr}, (ii) the (magneto)exciton size is much smaller than the electron and hole localization lengths in the in-plane disorder potential, and (iii) the (magneto)exciton binding energy (which vanishes at $P > P_{tr}$ for the magnetoexciton) is larger than the in-plane random potential fluctuations. Therefore our phase diagram is only valid for high-quality QW samples with a weak in-plane disorder.

Finally, one should note another practical limitation that restricts further the observation of the transition: the exciton size should be smaller than the average distance between the excitons: that is, the Mott criteria for the existence of a bound state.

IV. MAGNETOEXCITON DISPERSION RELATIONS AND EFFECTIVE MASSES IN FINITE $B_\perp$

In this section we compare the theoretical results with experimental data for indirect excitons in GaAs/$Al_{0.33}Ga_{0.67}$As CQW's with $d=11.5$ nm (see also Ref. 8). The principle of our experimental technique is based on our previous remark [see Eq. (4)] that a $\mathbf{B}_\parallel$ only shifts the magnetoexciton dispersion $E_X(\mathbf{P})$ by $(ed/c)\mathbf{B}_\parallel \times \hat{z}$ without changing its shape as illustrated in Fig. 9.

It is well known that the only free exciton states that can recombine radiatively are those inside the intersection between the dispersion surface $E_X(\mathbf{P})$ and the photon cone $E_{ph} = Pc/\sqrt{\varepsilon}$, called the radiative zone.[17] In GaAs structures the radiative zone corresponds to very small c.m. momenta $P/\hbar \leqslant K_0 \simeq E_g\sqrt{\varepsilon}/(\hbar c) \approx 2.7 \times 10^5$ cm^{-1}, where E_g is the semiconductor gap. Therefore as $B_\parallel$ increases the photon cone's intersection with the magnetoexciton dispersion surface varies and the energy of the excitons that are coupled to light, following the intersection, tracks the dispersion surface. Thus, by measuring the magnetoexciton photoluminescence (PL) energy as a function of the in-plane magnetic

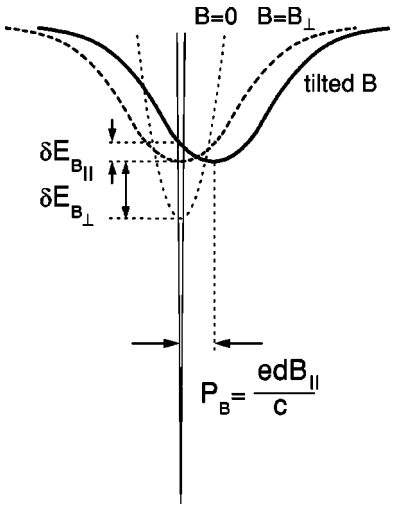

FIG. 9. Schematic of the indirect exciton dispersion at zero B, perpendicular B, and tilted B. The optically active exciton states are within the radiative zone determined by the photon cone.

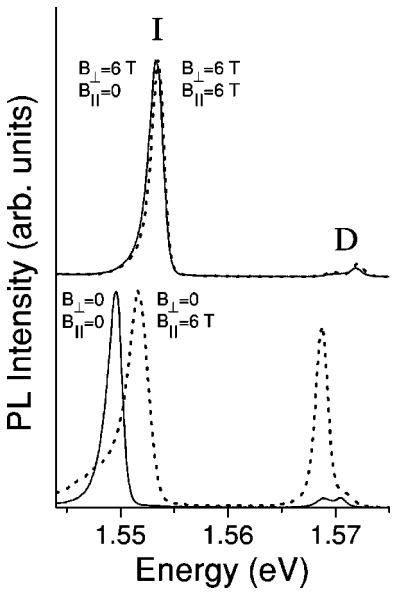

FIG. 10. PL spectra in magnetic fields $\mathbf{B}=B_{\|}\hat{x}+B_{\perp}\hat{z}$ for different perpendicular, $B_{\perp}$, and parallel, $B_{\|}$, components at $V_g=1$ V. The intensities are normalized.

field $B_{\|}$, one can determine the dispersion of the spatially indirect magnetoexciton.

We use a n^+-i-n^+ CQW heterostructure grown by molecular beam epitaxy (MBE). The i region consists of two 8-nm GaAs QW's separated by a 4-nm $Al_{0.33}Ga_{0.67}As$ barrier and surrounded by two 200-nm $Al_{0.33}Ga_{0.67}As$ barrier layers. The n^+ layers are Si-doped GaAs with $N_{Si}=5\times10^{17}$ cm^{-3}. The separation of the electron and hole layers in the CQW (the indirect regime) is achieved by the gate voltage V_g applied between the n^+ layers. V_g determines the external electric field in the $\hat{z}$ direction, $F=V_g/d_0$, where d_0 is the i-layer width, and is monitored externally. The shift of the indirect exciton energy with increasing gate voltage, $\Delta E_{PL}=eFd$, allows the determination of the mean interlayer separation in the indirect regime, $d=11.5$ nm, which is close to the distance between the QW centers.[18] For the CQW's studied here the shift induced by strong in-plane magnetic fields $K_B=(e/\hbar c)dB_{\|}$ is much larger than K_0. For example, at $B_{\|}=12$ T, $K_B\approx2.1\times10^6$ cm$^{-1}\sim8K_0$. Furthermore, for the narrow QW's the diamagnetic shift of the bottom of the bands is very small and can be neglected,[15] as confirmed by the negligible variation in the spatially direct transitions that we observe. Therefore, the peak energy of the indirect exciton PL is set by the energy of the radiative zone and for a parabolic dispersion is given as a function of $B_{\|}$ by $E_{P=0}=P_B^2/(2M_X)=e^2d^2B_{\|}^2/(2M_Xc^2)$; i.e., it is inversely proportional to the indirect (magneto)exciton mass M_X. The PL measurements were performed in tilted magnetic fields $\mathbf{B}=B_{\|}\hat{x}+B_{\perp}\hat{z}$ at $T=1.8$ K in a He cryostat with optical windows. Carriers were photoexcited by a HeNe laser at an excitation density 0.1 W/cm^2 and the PL spectra were measured by a charge-coupled-device (CCD) camera.

The basic features of the indirect magnetoexciton are the same as that of the direct magnetoexciton. However, because of the separation between the electron and hole layers, the indirect magnetoexciton binding energy and effective mass differ quantitatively from those of the direct magnetoexciton. As the interlayer separation d increases, the indirect magnetoexciton binding energy reduces, whereas its effective mass increases. In particular, in the high-magnetic-field limit $M_{Bd}=M_B[1+2^{3/2}d/(\pi^{1/2}l_B)]$ for $d\ll l_B$ and $M_{Bd}=M_B\pi^{1/2}d^3/(2^{3/2}l_B^3)$ for $d\gg l_B$.[7] The effective mass enhancement is easily explained using the electrostatic analogy: For separated layers the e-h Coulomb interaction is weaker than that within a single layer and changes only slightly for $\langle r\rangle\lesssim d$; this implies that $E_X(P)$ increases only slowly for $P\lesssim\hbar d/l_B^2$ or, in other words, that indirect magnetoexcitons have a large effective mass.

The spatially direct transitions (D) and the indirect transition (I) seen in Fig. 10 are identified by the PL kinetics and V_g dependence. The direct PL lines have short decay time and their positions practically do not depend on V_g, while the indirect exciton PL line has long decay time and shifts to lower energies with increasing V_g.[18] The upper and lower direct PL lines seen in Fig. 10 are related to the direct heavy-hole exciton X and the direct charged complexes X^+ and X^- which are composed of the carriers confined in the same QW.[19,20]

The shift of the indirect exciton PL line vs $B_{\|}$ gives the magnetoexciton dispersion presented in Fig. 11(a) for various $B_{\perp}$. The magnetoexciton effective mass at the band bottom is determined by the quadratic fits to the dispersion curves at small P. At $B_{\perp}=0$ the PL energy shift rate corresponds to $M_X=0.22m_0$, in good agreement with the calculated mass of heavy-hole exciton in GaAs QW's $\approx0.25m_0$ [$m_e=0.067m_0$ and in-plane heavy-hole mass $m_h=0.18\ m_0$ (Refs. 16 and 21)]. Drastic changes of the magnetoexciton dispersion are observed at finite $B_{\perp}$. The dispersion curves become significantly flat at small momenta as seen in Fig. 11. This corresponds to a strong enhancement of the magnetoexciton mass. Already at $B_{\perp}=4$ T the magnetoexciton mass has increased by about 3 times, and at higher

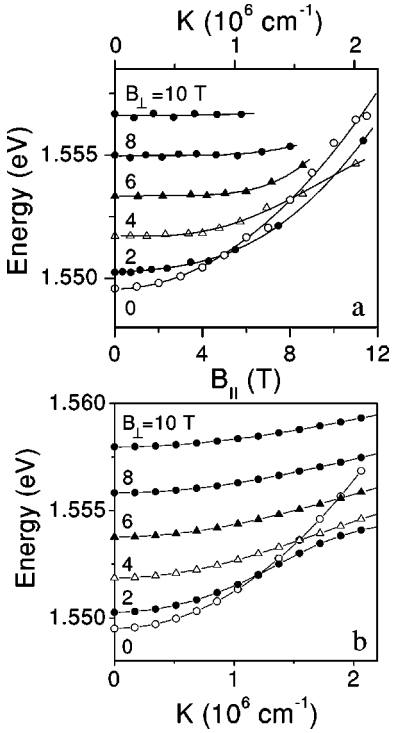

FIG. 11. (a) Measured and (b) calculated dispersions of an indirect magnetoexciton in $GaAs/Al_{0.33}Ga_{0.67}As$ CQW's with $d=11.5$ nm at $B_\perp=0$, 2, 4, 6, 8, and 10 T vs K ($B_\parallel$).

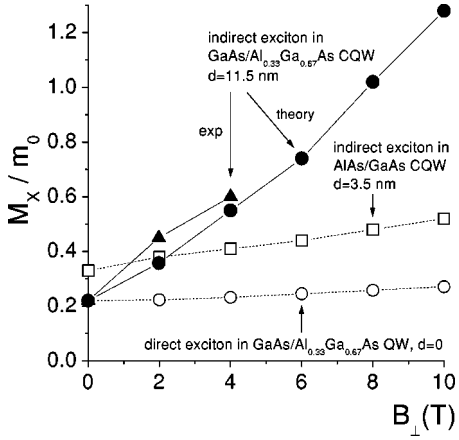

FIG. 12. Calculated effective masses of indirect (points) and direct (circles) excitons in $GaAs/Al_{0.33}Ga_{0.67}As$ CQW's with $d=11.5$ nm vs $B_\perp$. Triangles correspond to the experimental data for indirect excitons in $GaAs/Al_{0.33}Ga_{0.67}As$ CQW's with $d=11.5$ nm. Squares correspond to the calculated effective mass of an indirect exciton in AlAs/GaAs CQW with $d=3.5$ nm.

$B_\perp$ the dispersions become so flat that the scattering of the experimental points no longer allows precise determination of such large masses.

The experimental results are now compared with calculations of the magnetoexciton dispersion performed using the approach described in the previous sections. The results are shown in Fig. 11(b). We find that in a finite magnetic field the dispersion relation changes from a quadratic form at small P to the typical form for pure 2D magnetoexcitons at large P.[4,7] At the same time the effective mass which characterizes the dispersion at small P monotonically grows with $B_\perp$, Fig. 12. The calculated effective mass enhancement is in excellent agreement with the experimental data, with less than 10% discrepancy;[22] e.g., at $B_\perp=4$ T the measured magnetoexciton mass increase is 2.7 as compared to the theoretical value of 2.5 (see Fig. 12). The agreement still remains qualitatively good at high momenta (e.g. both experiment and theory show that at high P the magnetoexciton dispersions at finite $B_\perp$ become lower in energy than the exciton dispersion at $B_\perp=0$); however, the theory gives a rate of energy increase with momentum at high P slightly slower than the experiment. This quantitative difference does not change the general picture.

The good agreement between the theory (see the end of Sec. III) and the experimental data shows that the effects that we have not accounted for, such as finite QW width, complex band structure, spin related, and in-plane localization, cause only minor corrections to the magnetically induced effective mass enhancement. They are most likely too small to be observed in our experiment because of our choice of the experimental conditions. For our $GaAs/Al_xGa_{1-x}As$ CQW sample with narrow QW's, (1) the $L\neq 0$ effects are negligible in the wide range of in-plane magnetic fields such that $l_{B_\parallel}>L$ and (2) the complex band structure effects are negligible in the wide range of (magneto)exciton momenta such that $\delta E_{B_\parallel}\ll\delta E_{LH\text{-}HH}$, because of the large light-hole–heavy-hole band splitting, $\delta E_{LH-HH}=17$ meV.[20] For $GaAs/Al_xGa_{1-x}As$ QW's the electron and hole Zeeman splittings are small compared to the kinetic energy variation, so that the spin effects are negligible. Finally, our sample is of high quality, with very small in-plane disorder, so that localization effects are negligible. We should note, however, that the quantitative difference between experiment and theory for the rate of energy increase with momentum at the largest magnetoexciton momenta is unclear. The decrease in our experimental accuracy in the line positions at the highest $B_\parallel\gtrsim 10$ T, i.e., for the largest momenta $P/\hbar\gtrsim 1.8\times 10^6$ cm^{-1}, caused by the line broadening and the reduction in intensity, is insufficient to explain that difference.

We note that the observed large enhancement of the effective mass of the indirect exciton in magnetic fields is a single-exciton effect, unlike the well-known renormalization effects in neutral and charged e-h plasmas.[23] It has, however, very important effects on collective phenomena in the exciton system. In particular, the mass enhancement explains the disappearance of the stimulated exciton scattering and the transition from the highly degenerate to classical exciton gas with increasing magnetic field observed in Ref. 12.

In general, the magnetic field effect on the quantum degeneracy of the 2D exciton gas and the exciton condensation to the $P=0$ state has a complicated character which is briefly discussed below. There are the ''good'' effects induced by magnetic field which increase the quantum degeneracy and improve the critical conditions for the exciton condensation, and there are the ''bad'' effects which, on contrary, reduce the quantum degeneracy and suppress the exciton condensation.

The ''good'' effects of applying a magnetic field are the

following: (g1) It lifts the spin degeneracy g, resulting in the increase of the quantum degeneracy and of the exciton condensation critical temperature T_c which are both $\propto 1/g$. (g2) It increases the exciton binding energy, reduces the ground-state radius, and reduces screening. This increases the exciton stability and maximizes the exciton density which can be reached (limited by the Mott transition, which is determined by phase-space filling and screening, and inversely proportional to the square of the exciton radius[23]) and therefore increases the quantum degeneracy and T_c for high exciton densities. (g3) It results in the coupling between the exciton c.m. motion and internal structure. This coupling modifies the nature of the exciton condensation: At $B=0$ the exciton condensation is purely determined by the statistical distribution in momentum space of weakly interacting bosons (i.e., excitons),[24] while in the high-magnetic-field regime, due to the coupling, the e-h Coulomb attraction forces the excitons to the low-P states, and, therefore, the mean-field critical temperature T_c at which the quasicondensate appears[25,26] in the high-magnetic-field limit is determined (within the mean-field approximation valid at not very low LL filling factors) by the e-h pairing[27,28] similar to the case of the excitonic insulator[29] or Cooper pairs. According to the theory of Refs. 27 and 28, T_c in high magnetic fields is much higher than T_c at $B=0$ (see, for example, Fig. 1 of Ref. 14).

The ''bad'' effects of applying a magnetic field are the following: (b1) According to Refs. 30 and 31, in high magnetic fields the exciton condensate can be the ground state only if the separation between the layers is small $d \lesssim l_B$. For large d or small l_B the e-e and h-h rather than e-h correlations determine the ground state of spatially separated e and h layers. Therefore, magnetic fields such that $l_B \lesssim d$ should destroy the condensate. (b2) According to the previous sections the magnetic field increases the in-plane exciton mass M_X and, therefore, reduces the quantum degeneracy of the 2D exciton gas and T_c which are both $\propto 1/M_X$.[25,26,32] [Note that the Kosterlitz-Thouless transition temperature is also $\propto 1/M_X$ (Refs. 33 and 34).]

Some of the ''good'' and ''bad'' effects are crucially dependent on the interlayer separation d. In particular, small d is essential to maximize the g2 effect and g3 effect as the binding energy of indirect exciton is higher for the smaller d. Small d is also essential to overcome the b1 effect—namely, for the smaller d it is possible to reach higher magnetic fields before $l_B \sim d$. The results shown in Fig. 12 present the most important difference of the magnetic field effect on the quantum degeneracy of the exciton gas and on the exciton condensation for the systems with small and large d: For large d the magnetic field results in a huge enhancement of M_X, while for small d the mass enhancement is not significant. Therefore, a magnetic field could increase the quantum degeneracy of a 2D exciton gas and improve the critical conditions for the exciton condensation in systems of spatially separated electron and hole layers with small d and, vice versa, reduce the quantum degeneracy of the 2D exciton gas and suppress the exciton condensation in the systems of spatially separated electron and hole layers with large d. These results could explain the opposite effect of the magnetic field on the indirect excitons in AlAs/GaAs CQW's with $d = 3.5$ nm, where the magnetic field improves the critical conditions for the exciton condensation,[13,14] and on the indirect excitons in $GaAs/Al_{0.33}Ga_{0.67}As$ CQW's with $d = 11.5$ nm, where the magnetic field reduces the quantum degeneracy of the 2D gas of indirect excitons.[12]

V. CONCLUSION

In conclusion, we analyzed the dispersion relations and internal structures of the spatially indirect and direct excitons in single and coupled quantum wells in the entire range of magnetic field $B_\perp$. We revealed the existence of the sharp transition between the hydrogenlike exciton and magnetoexciton with increasing the exciton c.m. momentum P at a fixed weak $B_\perp$. At the transition the mean separation between the electron and hole $\langle r \rangle$ sharply rises and becomes $\langle r \rangle = cP/(eB_\perp)$ for the magnetoexciton. For the higher $B_\perp$ the transition smears out into the crossover and eventually disappears in the high-magnetic-field regime. The phase diagram describing an exciton in the magnetic-field–exciton momentum plane has been constructed. The calculated magnetoexciton dispersion relations and effective masses in finite $B_\perp$ are in an agreement with the experimental data for $GaAs/Al_{0.33}Ga_{0.67}As$ coupled quantum wells obtained by a new method for monitoring of the magnetoexciton dispersion relation using tilted magnetic fields. We have also discussed the impact of magnetic field and sample geometry on the condition for observing the exciton condensation.

The results of the work can be generalized to the case of three dimensions as well as to the case of any composite particles consisting of oppositely charged subparticles (i.e., atoms, molecules, etc.). An important manifestation of the effect is that such a composite particle is unstable in arbitrary small magnetic fields when its kinetic energy exceeds its binding energy.

ACKNOWLEDGMENTS

We acknowledge K.L. Campman and A.C. Gossard for providing the high-quality CQW samples used in our experiments. This work was supported by the Director, Office of Energy Research, Office of Basic Energy Sciences, Division of Material Sciences of the U.S. Department of Energy, under Contract No. DE-AC03-76SF00098 and by RFBR and INTAS grants.

APPENDIX: THE LIMITING CASE $B_\perp \to 0$

Our approach remains correct in the limiting case $B_\perp \to 0$. The Coulomb and magnetic minima of the ''effective potential'' $U_{eff}(r)$ are separated by $\rho_0 = cP/(eB_\perp)$. The smaller $|B_\perp|$ is, the larger ρ_0 is. In the small-field limit the Coulomb minimum is changed only slightly compared to the $B=0$ case, Eq. (6). The width of the e or h wave function in the zeroth LL is given by the magnetic length $l_B \sim 1/\sqrt{B_\perp}$ while the separation between the Coulomb minimum and the magnetic minimum $\rho_0 \sim 1/B_\perp$. Therefore, at $B_\perp \to 0$ the Coulomb minimum moves infinitely far away from the magnetic minimum and the overlap between the wave functions

located in the two minima becomes exponentially small. Therefore, these two states can be considered as independent candidates for the ground state of the system. The exponentially small overlap between the wave functions lifts the degeneracy of these states near the intersection point. The splitting of the spectrum is obtained by the diagonalization of the Hamiltonian calculated on the unperturbed wave functions of the LL, $\psi_{magn}(\mathbf{r}-\boldsymbol{\rho}_0)=(1/\sqrt{2\pi l_B})\exp[-r^2/(2l_B^2)]$, and the lowest bound state of the Coulomb potential, $\psi_{Coul}(r)=(\sqrt{2/\pi})a_{B2D}^{-1}\exp(-r/a_{B2D})$ [$a_{B2D}=\varepsilon\hbar^2/(2\mu e^2)$ is the 2D exciton Bohr radius]; i.e., the Hamiltonian is the 2×2 matrix

$$\hat{\mathcal{H}}=\begin{bmatrix} E_b & \delta \\ \delta & E_{magn} \end{bmatrix}.$$

And δ is proportional to the overlap between the wave functions:

$$\delta=\frac{1}{2}\hbar\omega_c\langle\psi_{Coul}|\psi_{magn}\rangle+\langle\psi_{Coul}|\hat{V}|\psi_{magn}\rangle$$

$$\propto\sqrt{\hbar\omega_c E_b}\exp\left(-\gamma\frac{E_b}{\hbar\omega_c}\right),$$

where $\gamma=\mu/M$.

Interestingly, the transition takes place at finite exciton momentum even at $B_\perp\to 0$. However, in the absence of a magnetic field, obviously there should be no transition in the system, which appears to be a contradiction. This, however, can be clarified as follows: When P becomes larger than P_{tr} the hydrogenlike bound state becomes metastable, but its lifetime, which is $\propto\delta^{-2}$, increases infinitely as $B_\perp\to 0$.

Note that the energy splitting between the lowest hydrogenlike level and the lowest LL at the intersection is equal to 2δ, Fig. 3.

[1] R.J. Elliott and R. Loudon, J. Phys. Chem. Solids **8**, 382 (1959); **15**, 196 (1960).

[2] H. Hasegawa and R.E. Howard, J. Phys. Chem. Solids **21**, 179 (1961).

[3] L.P. Gor'kov and I.E. Dzyaloshinskii, Zh. Éksp. Teor. Fiz. **53**, 717 (1967) [Sov. Phys. JETP **26**, 449 (1968)].

[4] I.V. Lerner and Yu.E. Lozovik, Zh. Éksp. Teor. Fiz. **78**, 1167 (1980) [Sov. Phys. JETP **51**, 588 (1980)].

[5] C. Kallin and B.I. Halperin, Phys. Rev. B **30**, 5655 (1984).

[6] D. Paquet, T.M. Rice, and K. Ueda, Phys. Rev. B **32**, 5208 (1985).

[7] Yu.E. Lozovik and A.M. Ruvinskii, Zh. Éksp. Teor. Fiz. **112**, 1791 (1997) [JETP **85**, 979 (1997)].

[8] L.V. Butov, C.W. Lai, D.S. Chemla, Yu.E. Lozovik, K.L. Campman, and A.C. Gossard, Phys. Rev. Lett. **87**, 216804 (2001).

[9] A.A. Gorbatsevich and I.V. Tokatly, Semicond. Sci. Technol. **13**, 288 (1998).

[10] L.V. Butov, A.V. Mintsev, Yu.E. Lozovik, K.L. Campman, and A.C. Gossard, Phys. Rev. B **62**, 1548 (2000).

[11] A. Parlangeli, P.C.M. Cristianen, J.C. Maan, I.V. Tokatly, C.B. Soerensen, and P.E. Lindelof, Phys. Rev. B **62**, 15 323 (2000).

[12] L.V. Butov, A.I. Ivanov, A. Imamoglu, P.B. Littlewood, A.A. Shashkin, V.T. Dolgopolov, K.L. Campman, and A.C. Gossard, Phys. Rev. Lett. **86**, 5608 (2001).

[13] L.B. Butov, A. Zrenner, G. Abstreiter, G. Böhm, and G. Weimann, Phys. Rev. Lett. **73**, 304 (1994).

[14] L.V. Butov and A.I. Filin, Phys. Rev. B **58**, 1980 (1998).

[15] F. Stern, Phys. Rev. Lett. **21**, 1687 (1968).

[16] G.E.W. Bauer and T. Ando, Phys. Rev. B **38**, 6015 (1988); B. Rejaei Salmassi and G.E.W. Bauer, *ibid.* **39**, 1970 (1989).

[17] J. Feldmann, G. Peter, E.O. Göbel, P. Dawson, K. Moore, C. Foxon, and R.J. Elliott, Phys. Rev. Lett. **59**, 2337 (1987).

[18] L.V. Butov, A.A. Shashkin, V.T. Dolgopolov, K.L. Campman, and A.C. Gossard, Phys. Rev. B **60**, 8753 (1999).

[19] V.B. Timofeev, A.V. Larionov, M. Grassi Alessi, M. Capizzi, A. Frova, and J.M. Hvam, Phys. Rev. B **60**, 8897 (1999).

[20] L.V. Butov, A. Imamoglu, K.L. Campman, and A.C. Gossard, Zh. Éksp. Teor. Fiz. **119**, 301 (2001) [JETP **92**, 260 (2001)]; *ibid.* [**92**, 752 (2001)].

[21] L.C. Andreani, A. Pasquarello, and F. Bassani, Phys. Rev. B **36**, 5887 (1987).

[22] The calculations use $M_X=0.22m_0$ at $B_\perp=0$, which was obtained from the measured exciton dispersion at $B_\perp=0$, and $d=11.5$ nm, which was obtained from the measured indirect exciton energy shift with applied electric field (Ref. 18). There is no fitting parameter in the calculations.

[23] S. Schmitt-Rink, D.S. Chemla, and D.A.B. Miller, Adv. Phys. **38**, 89 (1989).

[24] L.V. Keldysh and A.N. Kozlov, Zh. Éksp. Teor. Fiz. **54**, 978 (1968) [Sov. Phys. JETP **27**, 521 (1968)].

[25] V.N. Popov, Theor. Math. Phys. **11**, 565 (1972); P.N. Brusov and V.N. Popov, *Superfluidity and Collective Properties of Quantum Liquids* (Nauka, Moscow 1988), Chap. 6.

[26] D.S. Fisher and P.C. Hohenberg, Phys. Rev. B **37**, 4936 (1988).

[27] I.V. Lerner and Yu.E. Lozovik, Pis'ma Zh. Éksp. Teor. Fiz. **27**, 467 (1978) [JETP Lett. **27**, 467 (1978)]; J. Low Temp. Phys. **38**, 333 (1980); Zh. Éksp. Teor. Fiz. 80, 1488 (1981) [Sov. Phys. JETP **53**, 763 (1981)].

[28] Y. Kuramoto and C. Horie, Solid State Commun. **25**, 713 (1978).

[29] L.V. Keldysh and Yu.E. Kopaev, Fiz. Tverd. Tela (Leningrad) **6**, 2791 (1964) [Sov. Phys. Solid State **6**, 6219 (1965)].

[30] D. Yoshioka and A.H. MacDonald, J. Phys. Soc. Jpn. **59**, 4211 (1990).

[31] X.M. Chen and J.J. Quinn, Phys. Rev. Lett. **67**, 895 (1991).

[32] W. Ketterle and N.J. Van Drutten, Phys. Rev. A **54**, 656 (1996).

[33] J.M. Kosterlitz and D.J. Thouless, J. Phys. C **6**, 1181 (1973).

[34] Yu.E. Lozovik and O.L. Berman, JETP Lett. **64**, 573 (1996).